Inorganic Chemistry

ARTICLE

pubs.acs.org/IC

A Highly Distorted Open-Shell Endohedral Zintl Cluster: $[Mn@Pb_{12}]^{3-}$

Binbin Zhou, Tobias Krämer, Amber L. Thompson, John E. McGrady,* and Jose M. Goicoechea*

Department of Chemistry, Inorganic Chemistry Laboratory, University of Oxford, South Parks Road, Oxford OX1 3QR, U.K.

Ⓢ *Supporting Information*

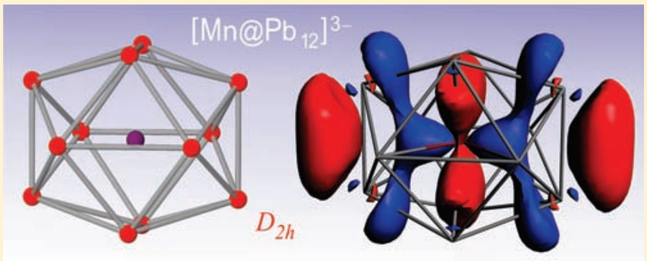

ABSTRACT: Reaction of an ethylenediamine (en) solution of K_4Pb_9 and 2,2,2-crypt (4,7,13,16,21,24-hexaoxa-1,10-diazabicyclo-[8.8.8]hexacosane) with a tetrahydrofuran (THF) solution of $Mn_3(Mes)_6$ (Mes = 2,4,6-trimethylphenyl) yielded the anionic cluster $[Mn@Pb_{12}]^{3-}$. This species was observed in the positive and negative ion-mode electrospray mass-spectra of the crude reaction mixture. The crystalline samples obtained from such solutions allowed us to confirm the composition of the sample as $[K(2,2,2\text{-crypt})]_3[Mn@Pb_{12}]\cdot 1.5en$ (**1**). Because of numerous issues related to crystal sample quality and crystallographic disorder a high-quality crystal structure solution could not be obtained. Despite this, however, the data collected permit us to draw reasonable conclusions about the charge and connectivity of the $[Mn@Pb_{12}]^{3-}$ cluster anion. Crystals of **1** were further characterized by elemental analysis and electron paramagnetic resonance (EPR). Density Functional Theory (DFT) calculations on such a system reveal a highly distorted endohedral cluster anion, consistent with the structural distortions observed by single crystal X-ray diffraction. The cluster anions are considerably expanded compared to the 36-electron closed-shell analogue $[Ni@Pb_{12}]^{2-}$ and, moreover, exhibit significant low-symmetry distortions from the idealized icosahedral (I_h) geometry that is characteristic of related endohedral clusters. Our computations indicate that there is substantial transfer of electron density from the formally Mn(−I) center to the low-lying vacant orbitals of the $[Pb_{12}]^{2-}$ cage.

1. INTRODUCTION

The observation that nonatetrelide group 14 Zintl anions, $[E_9]^{4-}$ (E = Ge, Sn, Pb), can react with sources of "naked" (substituent-free) metal atoms to give metal-centered (endohedral) clusters has been reported on a handful of occasions over the past six years.[1] The earliest of these studies, reported by Eichhorn and co-workers, found that reactions between $[Pb_9]^{4-}$ and the closed-shell d^{10} metal reagent $[Pt(PPh_3)_4]$ (Ph = C_6H_5), could be used to synthesize the transition metal-centered cluster anion $[Pt@Pb_{12}]^{2-}$.[2] Related chemistry utilizing different transition metal reagents ultimately gave rise to a homologous series of isostructural and isoelectronic icosahedral clusters: $[M@Pb_{12}]^{2-}$ (M = Ni, Pd, Pt).[3] More recently, the isoelectronic iridium-centered species $[Ir@Sn_{12}]^{3-}$ has been synthesized by Fässler and co-workers.[4] All of these species show almost perfect icosahedral symmetry, with the M-E and E-E bond lengths dispersed over a narrow range around the mean. Prior to this research, there had been a handful of reports on the observation of $[M@Pb_{12}]^{x\pm}$ clusters in mass spectrometric experiments, including a $[Co@Pb_{12}]^{-}$ anion,[5] isoelectronic with the title compound, and $[Mn@Pb_{12}]^{x+}$ ($x = 0, 1$).[6] In the former case the authors proposed a perfect icosahedral structure for the endohedral anion.

Endohedral Zintl ion clusters are not restricted to 12-vertex polyhedra, and "spherical" deltahedral clusters with interstitial atoms have also been isolated with 9 ($[Ni@Ge_9]^{3-}$, $[Cu@E_9]^{3-}$ (E = Sn, Pb)),[7,8] and 10 ($[Ni@Pb_{10}]^{2-}$) cage atoms.[3,9] The bicapped square antiprismatic structure of the latter makes a striking contrast with the Co and Fe analogues of germanium, $[M@Ge_{10}]^{3-}$ (M = Co, Fe), which adopt remarkable nondeltahedral pentagonal prismatic structures.[10] Larger nonspherical metal-centered deltahedra such as $[Ni(Ni@Ge_9)_2]^{4-}$,[11] $[Pd_2@Ge_{18}]^{4-}$,[12] $[Pd_2@Sn_{18}]^{4-}$, and $[Pt_2@Sn_{17}]^{4-}$,[13,14] all of which contain interstitial d^{10} metal atoms, have also been reported in the literature.

The ability of "empty" group 14 Zintl clusters to undergo functionalization reactions with organic and metal−organic fragments has been relatively well documented,[15,16] as has the possibility of oxidative coupling of such clusters to yield oligomers and polymers.[17] In related studies, metal-linked macromolecular species based on $[E_9]^{4-}$ building blocks such as $[\{Ni(CO)_2\}_2(Si_9)_2]^{8-}$,[18] $[Hg(Ge_9)]_\infty^{2-}$,[19] $[Hg(Ge_9)_2]^{2-}$,[20] $[Hg_3(Ge_9)_4]^{10-}$,[21] $[Au_3(Ge_9)_2]^{5-}$,[22] $[Au_3Ge_{45}]^{9-}$,[23] $[Hg(Sn_9)_2]^{6-}$,[24] and $[Cd_2(Pb_9)_2]^{6-}$ have also been reported.[25] The use of group 14 Zintl cluster anions as precursors to novel nanomaterials has recently been noted in the literature, highlighting feasible applications which may have some technological relevance.[26] By analogy, similar reactions of endohedral metal clusters could be used to generate heteroatomic cluster oligomers, polymers, and nanostructured solids.

It is significant that the majority of the endohedral group 14 clusters isolated to date exhibit nuclearities greater than those of the nonatetrelide starting materials. This implies that such

Received: February 17, 2011
Published: August 04, 2011

reactions proceed via nonstoichiometric pathways resulting in extensive decomposition of the nine-atom starting materials. This fragmentation is particularly prominent for the heavier congeners of group 14, the reactions of which frequently yield elemental tin or lead as byproducts. The mechanism by which these clusters undergo extensive cluster fragmentation and reassembly is perhaps the greatest enigma that needs to be resolved in this area of main-group chemistry. Similar reactions involving cluster fragmentation and reassembly have also been found to yield "empty" and functionalized cluster anions such as $[Pb_{10}]^{2-}$, $[Ge_8Fe(CO)_3]^{3-}$, or $[Ge_{10}Mn(CO)_4]^{3-}$,[27–29] with nuclearities different to those of the nine-atom precursors.

All the endohedral deltahedra described in the previous paragraphs share a common closed-shell d^{10} configuration at the metal center. In the case of $[M@Pb_{12}]^{2-}$ (M = Ni, Pd, Pt) the interstitial metal atoms are zerovalent (Ni(0), Pd(0), or Pt(0)),[2,3] while in the case of the $[Ir@Sn_{12}]^{3-}$ anion, Fässler and co-workers have argued for a *closo*-$Sn_{12}{}^{2-}$ cluster encapsulating an iridium center in the −I oxidation state.[4] As such, all of these $[M@E_{12}]^{x-}$ cluster anions can be rationalized as *closo*-clusters with a total electron count of 26 (36 if the electrons from the interstitial metal are taken into account), in accordance with the Wade/Mingos rules for bonding in metal clusters.[30] Such a *closo* arrangement is consistent with the near perfect icosahedral geometries with equivalent M-E and E-E bond lengths exhibited in each case. In this paper we report the isolation of an open-shell member of the icosahedral $[M@Pb_{12}]^{x-}$ family, $[Mn@Pb_{12}]^{3-}$, formed by the reaction of the group 14 nine-atom cluster anion $[Pb_9]^{4-}$ with $Mn_3(Mes)_6$. The $[Mn@Pb_{12}]^{3-}$ cluster anion was identified by electrospray mass-spectrometry measurements of crude reaction mixtures (and later from solutions of the solids obtained from such mixtures). The $[Mn@Pb_{12}]^{3-}$ anion can be isolated as a $[K(2,2,2\text{-crypt})]^+$ salt in $[K(2,2,2\text{-crypt})]_3[Mn@Pb_{12}]\cdot 1.5en$ (**1**). Crystalline samples of **1** allowed for the collection of X-ray diffraction data which permit reasonable conclusions to be drawn about the charge and connectivity of the cluster anion. The solid was further characterized by electron paramagnetic resonance (EPR) and elemental analysis. The cluster anions present in **1** exhibit significant structural distortions away from the ideal icosahedral (I_h) structure adopted by the closed shell analogues $[M@Pb_{12}]^{2-}$ (M = Ni, Pd, Pt) and $[Ir@Sn_{12}]^{3-}$.[2–4] Density Functional Theory suggests that the distortion is a consequence of significant transfer of charge from the formally Mn(−I) center to the antibonding orbitals of the *closo*-$[Pb_{12}]^{2-}$ cage.

2. EXPERIMENTAL SECTION

General Synthetic Methods. All reactions and product manipulations were carried out under an inert atmosphere using standard Schlenk-line or glovebox techniques (MBraun UNIlab glovebox maintained at <0.1 ppm H_2O and <0.1 ppm O_2). The intermetallic precursor K_4Pb_9 was synthesized according to a previously reported synthetic procedure from a stoichiometric mixture of the elements (K: 99.95%, Aldrich; Pb: 99.99%, Strem).[31] $Mn_3(Mes)_6$ was synthesized using a literature-reported method.[32] 2,2,2-Crypt (4,7,13,16,21,24-hexaoxa-1,10-diazabicyclo[8.8.8]hexacosane; 99+%, Merck) was used as received after careful drying under vacuum. Tetrahydrofuran (THF; 99.9%, Rathburn), Et_2O (99.9%, Fisher) and dimethylformamide (DMF; 99.9%, Rathburn) were purified using an MBraun SPS-800 solvent system. Ethylenediamine (en; 99%, Aldrich) was distilled over sodium metal. All solvents were stored under argon in gastight ampules. In addition, THF and Et_2O were stored over activated 3 Å molecular sieves (Acros).

Synthesis of $[K(2,2,2\text{-crypt})]_3[Mn@Pb_{12}]\cdot 1.5en$ (1). A mixture of K_4Pb_9 (150 mg, 0.074 mmol) and 2,2,2-crypt (85 mg, 0.226 mmol) were dissolved in approximately 3 mL of ethylenediamine giving rise to a dark green solution. To this solution, a pale yellow solution of $Mn_3(Mes)_6$ (22 mg, 0.025 mmol) in THF (1.5 mL) was added dropwise over the course of 10 min. The reaction mixture was stirred for 1 h, filtered into an ampule under an inert atmosphere, and the filtrate layered with Et_2O for crystallization. After several days, thin black plate-like crystals of $[K(2,2,2\text{-crypt})]_3[Mn@Pb_{12}]\cdot 1.5en$ were obtained alongside some metallic decomposition. Anal. Calcd. for $[K(2,2,2\text{-crypt})]_3[Mn@Pb_{12}]\cdot 1.5en$ ($C_{57}H_{120}K_3MnN_9O_{18}Pb_{12}$): C, 17.64; H, 3.12; N, 3.25. Found: C, 17.47; H, 2.99; N, 2.93. ES− MS: *m/z* 1035.7 $[Pb_5]^-$, 1074.7 $\{K[Pb_5]\}^-$, 1452.1 $\{[K(2,2,2\text{-crypt})][Pb_5]\}^-$, 2072.6 $[Pb_{10}]^-$, 2487.8 $[Pb_{12}]^-$, 2541.4 $[Mn@Pb_{12}]^-$, 2902.7 $\{[K(2,2,2\text{-crypt})][Pb_{12}]\}^-$, 2957.5 $\{[K(2,2,2\text{-crypt})][Mn@Pb_{12}]\}^-$. ES+ MS: *m/z* 2283.3 $\{[K(2,2,2\text{-crypt})]_3[Pb_5]\}^+$, 3318.1 $\{[K(2,2,2\text{-crypt})]_3[Pb_{10}]\}^+$, 3733.0 $\{[K(2,2,2\text{-crypt})]_3[Pb_{12}]\}^+$, 3788.1 $\{[K(2,2,2\text{-crypt})]_3[Mn@Pb_{12}]\}^+$.

Structure Determination. Single crystal X-ray diffraction data for **1** were collected on an Enraf-Nonius Kappa CCD diffractometer and using synchrotron radiation on a CrystalLogic Kappa (3 circle) diffractometer at beamline I19 (EH1) at the Diamond Light Source, Didcot. Crystals were selected under Paratone-N oil, mounted on MiTeGen loops and quench-cooled using an open flow N_2 cooling device.[33] The laboratory data were collected at 150 K using graphite monochromated Mo K_α radiation and processed using the DENZO-SMN package, including unit cell parameter refinement and interframe scaling (which was carried out using SCALEPACK within DENZO-SMN).[34] The synchrotron data were collected at the zirconium edge ($\lambda = 0.6889$ Å) and were processed using CrystalClear-SM Expert 2.0 r4.[35] Structure **1a** (from laboratory data) was solved by direct methods and refined on F^2 using the SHELX-97 package.[36] Structure **1b** (synchrotron data) was solved by refinement of the structure determined from **1a**. Structure determination was handicapped by the fact that the crystals were highly air- and moisture-sensitive. The small, metallic-black, needle-shaped crystals grow from a dark purple solution making identifying a good quality specimen, and collecting data without damage to the crystal extremely challenging. Scattering was dominated by the clusters, and the presence of pseudosymmetry arising from the cluster anions (but broken by the light atoms) also complicated matters leading to difficulties with data processing. The strong, low angle reflections were found to saturate the detector while weaker reflections were poorly determined, which coupled with the shape of the crystals, also gave problems scaling raw frames and correcting for absorption.

A full discussion of the details regarding the structural determination of **1a** and **1b** are provided in the Supporting Information. Because of the similarities between the two data sets only sample **1a** is discussed in the manuscript.

Computational Methods. All calculations described in this paper were performed with the Amsterdam Density Functional package (ADF2009.01).[37] The TZ2P Slater-type basis set of triple-ζ zeta quality, extended with two polarization functions, was used to describe Mn and Pb. Electrons in orbitals up to and including 2p for Mn and 4d for Pb were considered part of the core and treated in accordance with the frozen core approximation (Mn.2p and Pb.4d). All calculations employed the Local Density Approximation (LDA)[38] to the exchange potential, along with the local exchange-correlation potential of Vosko, Wilk and Nusair (VWN)[39] and gradient corrections to nonlocal exchange and correlation proposed by Becke and Perdew (BP86).[40] All calculations were unrestricted. Relativistic effects were incorporated using the Zeroth Order Relativistic Approximation (ZORA).[41] The presence of cations in the crystal lattice was modeled by surrounding the clusters with a continuum dielectric model (COSMO).[42] The chosen dielectric constant ε = 78.4 corresponds to that of water, although structural parameters are not strongly dependent on this choice. All structures were optimized using the gradient algorithm of Versluis and Ziegler.[43] We note that I_h point symmetry is not supported in ADF, but by using an appropriate subgroup (in this case D_{5d}) and imposing a symmetric electron density distribution with 1 spin-α and 3/5 spin-β electrons in each of the five highest lying orbitals with the symmetries of the 3d set (a_{1g}, e_{1g}, e_{2g}), it is possible to converge on the I_h-symmetric geometries discussed below. Stationary points were characterized by analysis of their harmonic frequencies: true minima and transition states have 0 and 1 imaginary frequencies, respectively. Frequencies were computed by numerical differentiation of energy gradients in slightly displaced geometries.

Additional Characterization Techniques. Continuous Wave Electron Paramagnetic Resonance (CW EPR) experiments were performed using an X-band Bruker BioSpin GmbH EMX spectrometer equipped with a high sensitivity Bruker probe head and a low-temperature Oxford Instruments CF935 helium-flow cryostat. Experiments were conducted with 2−10 mW microwave power, 0.1 mT modulation amplitude and a modulation frequency of 100 kHz. The magnetic field was calibrated at room temperature with an external 2,2-diphenyl-1-picrylhydrazyl standard (g = 2.0036). Spectra were recorded on approximately 2 mg of a solid sample in flame-sealed quartz capillaries.

Positive and negative ion mode electrospray mass spectra were recorded from DMF solutions (10−20 μM) on a Masslynx LCT Time of Flight mass spectrometer with a Z-spray source (150 °C source temperature, 200 °C desolvation temperature, 2.4 kV capillary voltage and 25 V cone voltage). The samples were introduced directly with a 1 mL SGE syringe and a syringe pump at 0.6 mL/h.

CHN elemental analyses were performed on 5 mg samples submitted under vacuum in flame-sealed Pyrex ampules.

3. RESULTS AND DISCUSSION

Reaction of an en solution of K_4Pb_9 and 2,2,2-crypt with a THF solution of $Mn_3(Mes)_6$ gave rise to a dark purple/black mixture, along with considerable amounts of metallic decomposition. Filtration of the reaction mixture under an inert atmosphere yielded a purple/black solution containing the $[Mn@Pb_{12}]^{3-}$ cluster anion. This reaction proceeds via reductive cleavage of the M-C bonds in $Mn_3(Mes)_6$ by the solvated electrons present in the K_4Pb_9 solution and yields mesitylene as a side-product. Similar reactions with other low coordinate organometallics have proven a viable route to endohedral and *exo*-functionalized Zintl cluster anions and appear to be very sensitive to the nature of the organometallic reagents employed.[1] The presence of the cluster anion in solution was confirmed by electrospray mass-spectrometric measurements of the crude reaction mixture. It was later observed that the product of the reaction could be precipitated out of solution by addition of toluene, which gave rise to a dark reddish-black solid. Electrospray mass-spectrometry measurements of DMF solutions of the resulting solids also confirm the presence of the cluster anion.

As is frequently the case with electrospray studies of anionic Zintl ions, the negative ion mode spectrum revealed peaks arising from clusters with reduced charges, a result of the oxidation of the parent polyanion during ionization. Furthermore, there is also evidence of ion pairing between anions and charge balancing cations. The negative ion mode spectrum of DMF solutions of **1** revealed mass envelopes corresponding to $[Mn@Pb_{12}]^{-}$ (m/z = 2541.4) and $\{[K(2,2,2\text{-crypt})][Mn@Pb_{12}]\}^{-}$ (m/z = 2957.5). These mass-envelopes are pictured in Figure 1. The positive ion mode spectrum of the sample revealed a peak corresponding to $\{[K(2,2,2\text{-crypt})]_3[Mn@Pb_{12}]\}^{+}$ at m/z = 3788.1. During the course of these studies it was observed that the $[Mn@Pb_{12}]^{3-}$ cluster anion is relatively unstable in DMF at low concentrations. Electrospray mass-spectra of DMF solutions of **1** showed evidence of other well know Zintl anions such as $[Pb_5]^{2-}$ and $[Pb_{10}]^{2-}$ with the relative concentration of $[Mn@Pb_{12}]^{3-}$ decreasing the longer these were left to stand.

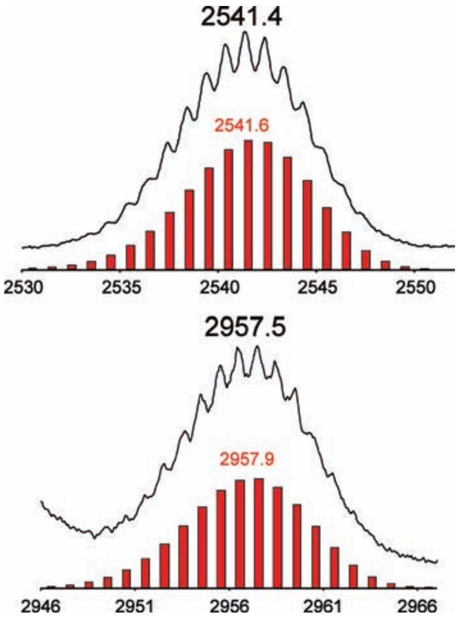

Figure 1. Negative ion-mode electrospray mass-envelopes corresponding to $[Mn@Pb_{12}]^{-}$ (top) and $\{[K(2,2,2\text{-crypt})][Mn@Pb_{12}]\}^{-}$ (bottom). Recorded experimental data are given in black with the calculated isotopic distributions in red.

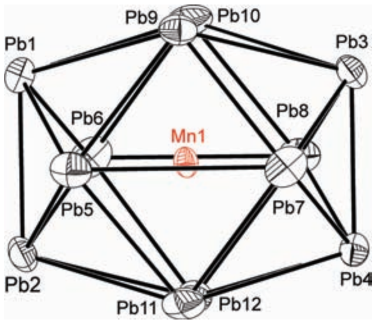

Figure 2. Thermal ellipsoid plot of one of the three crystallographically unique $[Mn@Pb_{12}]^{3-}$ cluster anions (A1) present in **1a**. Anisotropic displacement ellipsoids are pictured at the 50% probability level.

Crystals of the $[Mn@Pb_{12}]^{3-}$ anion could be obtained by layering the aforementioned en/THF reaction mixtures with Et_2O and leaving the mixture to diffuse over the course of several days. This method produced very small, highly anisotropic, black crystals. The collection of high-quality single-crystal X-ray diffraction data proved problematic. Despite numerous complications with the crystalline samples (detailed in the Supporting Information), we were eventually able to obtain two data sets of reasonable quality. All attempts to crystallize the $[Mn@Pb_{12}]^{3-}$ cluster anion from different solvent mixtures and/or using alternative sequestering agents proved unsuccessful. Full details

Table 1. Selected X-ray Data Collection and Refinement Parameters for $[K(2,2,2\text{-crypt})]_3[Mn@Pb_{12}]\cdot 1.5en$ (**1a**)

compound	**1a**
formula	$C_{57}H_{120}K_3MnN_9O_{18}Pb_{12}$
Fw	3878.14
space group, Z	$P2_1/c$, 8
a (Å)	17.4420(1)
b (Å)	23.2970(2)
c (Å)	50.4120(4)
α (deg)	90
β (deg)	110.230(1)
γ (deg)	90
V (Å^3)	19221.1(3)
ρ_{calc} (g cm^{-3})	2.680
radiation, λ (Å),	Mo K$_\alpha$, 0.71073,
temp (K)	150(2)
μ (mm^{-1})	21.246
reflections collected	41527
independent reflections	32162
R(int) (%)	8.43
R1/wR2,[a] $I > 2\sigma(I)$ (%)	7.83/12.77
R1/wR2,[a] all data (%)	12.20/13.80

[a] $R1 = [\Sigma||F_o| - |F_c||]/[\Sigma|F_o|]$; $wR2 = \{[\Sigma w(F_o^2 - F_c^2)^2]/[\Sigma w(F_o^2)^2]\}^{1/2}$.

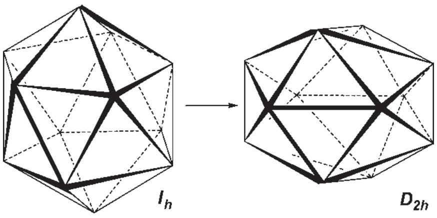

Figure 3. Schematic representation of the distortion of an I_h geometry to yield a D_{2h} cluster. This is achieved via compression/elongation along two orthogonal 2-fold rotation axes of the icosahedron.

of data collection and refinement parameters are provided in the Supporting Information. The quality of these data sets clearly remains less than ideal and as a result some caution must be employed when discussing absolute bond metrics, particularly those associated with the lighter elements in the 2,2,2-crypt ligands. Nevertheless, the data sets are sufficient to draw reliable conclusions regarding the composition, charge, connectivity, and geometries of the all-important trianionic cluster units (Figure 2). Moreover, we believe that the analysis of this bond metric data over several closely related units provides a statistically meaningful picture of the gross distortion in this remarkable species. Selected details of data collection and refinement parameters are provided in Table 1.

Table 2. Mn−Pb Distances for the Cluster Anion in 1a Which Is Not Located on a Crystallographic Inversion Center

Mn−Pb distances	**1a**
Mn1 Pb1	3.272(4)
Mn1 Pb2	3.274(4)
Mn1 Pb3	3.296(4)
Mn1 Pb4	3.308(4)
Mn1 Pb5	3.099(3)
Mn1 Pb6	3.080(4)
Mn1 Pb7	3.083(4)
Mn1 Pb8	3.112(4)
Mn1 Pb9	2.869(3)
Mn1 Pb10	2.886(4)
Mn1 Pb11	2.876(4)
Mn1 Pb12	2.891(3)

Crystals of **1** contain three crystallographically unique cluster anions in their asymmetric units. Of the three, one is entirely unconstrained by crystallographic symmetry while the foci (i.e., the interstitial manganese atoms) of the two remaining clusters are located on crystallographic inversion centers. All of the cluster anions present in **1** exhibit pronounced structural distortions away from the icosahedral (I_h) geometry that is common to the closed-shell analogues, $[M@Pb_{12}]^{2-}$ (M = Ni, Pd, Pt) and $[Ir@Sn_{12}]^{3-}$.[2−4] The nature of the distortion is quite specific and common to all the crystallographically independent cluster units. In the cluster that is unconstrained by crystallographic symmetry, elongation and compression along mutually orthogonal C_2 axes of the icosahedra leads to a D_{2h}-symmetric structure (Figure 3). An analysis of the radial distribution functions of the Mn−Pb and Pb−Pb interatomic distances is consistent with this kind of distortion (see Supporting Information for full details). In the units whose foci lie on inversion centers compression along an icosahedral 2-fold rotation axis is accompanied by a small elongation along a 5-fold, generating a C_{2h}-symmetric structure. The distortion from D_{2h} symmetry is, however, relatively minor (see Supporting Information for full details). The structural parameters for the crystallographically unconstrained cluster present in **1a** (with approximate D_{2h} symmetry) are presented in Table 2. The twelve Mn−Pb bond distances fall into three quite distinct and rather narrow ranges. The four shortest lie around the waist of the cluster (Mn−Pb9, 10, 11 and 12: ∼2.9 Å), while the longest are associated with the poles of the prolate ellipsoid (Mn−Pb1, 2, 3, 4: ∼3.3 Å). The four intermediate distances, to Pb5, 6, 7, and 8, are centered on ∼3.1 Å. The Pb−Pb separations also span a far larger range than the closed-shell analogues, from two very short distances (Pb1−Pb2, Pb3−Pb4: ∼3.1 Å) to two very much longer ones parallel to the long axis (Pb5−Pb7, Pb6−Pb8, ∼3.6 Å). The average Pb−Pb bond distance of 3.247 Å is substantially longer than that in the nickel analogue (3.078 Å). The inherent disorder present in the C_{2h}-symmetric clusters that are centered on the crystallographic inversion centers makes the analysis of bond lengths more complicated, but the data collected in Table 3, which represent the average over all of the clusters present in **1a**, shows that a statistically meaningful variance of the Mn−Pb and Pb−Pb bonds is common to all cluster units. Moreover, the variance is notably larger than in any of the analogous closed-shell systems (Table 3).

Graphical evidence of this structural distortion and an in-depth analysis of bond metrics are provided in the Supporting Information. In Section 5 we analyze the origins of this distortion in terms of the electronic structure of the cluster.

4. EPR SPECTROSCOPY

The EPR spectrum of a solid sample of **1** reveals a strong broad resonance at room temperature with a g value of 2.0095 (Figure 4). This spectrum confirms the paramagnetic character of the cluster anion and is presumably broadened because of spin−orbit coupling with the atoms of the cluster

Table 3. Summary of Structural Data for the $[M@E_{12}]^{x-}$ (M = Ni–Pt, x = 2; M = Mn, Ir, x = 3) Cluster Anions

		M-E distances			E-E distances		
cluster	radii of M (Å)[a]	average (Å)	range (Å)	variance[b] $\sigma^2 \times 10^{-3}$	average (Å)	range (Å)	variance $\sigma^2 \times 10^{-3}$
$[Ni@Pb_{12}]^{2-}$[c]	1.24(4)	3.001	0.112	1.3	3.078	0.028	0.14
$[Pd@Pb_{12}]^{2-}$[c]	1.39(6)	3.033	0.112	1.1	3.189	0.080	0.33
$[Pt@Pb_{12}]^{2-}$[c]	1.36(5)	3.058	0.003	0.004	3.216	0.214	3.1
$[Ir@Sn_{12}]^{3-}$[d]	1.41(6)	2.906	0.076	0.7	3.074	0.127	1.0
$[Mn@Pb_{12}]^{3-}$[e]	1.39(5)	3.063	0.630	23.67	3.223	1.104	26.6

[a] Data from ref 44. [b] Variance defined as: $\sigma^2 = [\Sigma_{i=1}^{N}(x_i - \bar{x})^2]/(N-1)$. [c] Data from ref 2. [d] Data calculated from crystallographic supporting material provided for ref 4. [e] Data calculated for all distances including symmetry-related values in **1a**.

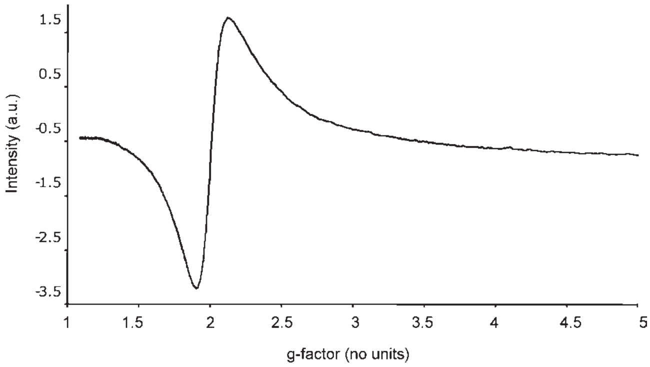

Figure 4. X-band (9.3896 GHz) CW EPR spectrum of a solid sample of **1** recorded at 296 K.

cage and/or fast relaxation effects. The spectrum reveals no evidence of a weak spin-forbidden resonance at half field which would arise because of a triplet ground state; however, this may well be lost in the baseline because of the broad nature of the resonance. The g-value and broad nature of the EPR resonance we observe is consistent with that previously reported for other paramagnetic lead clusters such as $[Pb_9]^{3-}$.[45] Attempts to record the spectrum of **1** in solution, and thus observe hyperfine coupling with ^{207}Pb isotopes, were significantly hampered by the poor stability of the cluster anion. The high dilution required for solution-phase EPR spectroscopy resulted in sample decomposition (presumably because of the presence of trace amounts of moisture in the solvent and/or the long-term instability of the cluster anion in solution). As a result, no solution-phase spectra could be obtained.

5. ELECTRONIC STRUCTURE ANALYSIS

We noted in the introduction that the electronic structure of the closed shell clusters $[Ni@Pb_{12}]^{2-}$, $[Pd@Pb_{12}]^{2-}$, $[Pt@Pb_{12}]^{2-}$, and $[Ir@Sn_{12}]^{3-}$ can be understood in terms of a formal d^{10} electronic configuration (Ni/Pd/Pt(0), Ir(−I)) and a total skeletal electron count of 26 (or 36 if the interstitial metal electrons are included). There have been numerous theoretical studies of both "empty" and endohedral ten- and twelve-vertex group 14 cluster anions.[46−63] In the context of the current study, the recent work of Deng and co-workers on neutral $M@Pb_{12}$ complexes of the first row transition series is particularly relevant. $Mn@Pb_{12}$ was reported to have a sextet ground state with 4.34 unpaired electrons on the Mn center, consistent with a $Mn(II)@Pb_{12}^{2-}$ formulation.[63] Indeed, Kumar and co-workers have referred to the germanium and tin analogues, $Mn@E_{12}$ (E = Ge, Sn) as a "magnetic superatoms",[51] where the high local moment at the metal center is shielded from the environment by the E_{12} cluster. The neutral nickel analogue, $Ni@Pb_{12}$, formally isoelectronic with $[Mn@Pb_{12}]^{3-}$, was reported to have a triplet ground state and only minor deviations from icosahedral symmetry. The very weak Jahn–Teller distortion in $Ni@Pb_{12}$ contrasts dramatically with the strong prolate distortion observed in $[Mn@Pb_{12}]^{3-}$, an observation that has prompted us to use density functional theory to explore the origins of the differences between the two isoelectronic species.

Given the rather low quality of the X-ray data, we have conducted an exhaustive survey of the potential energy surface of the $[Mn@Pb_{12}]^{3-}$ anion to identify all possible isomers. This analysis reveals two almost iso-energetic low-lying stationary points (Table 4), one with D_{3d} symmetry, the other D_{2h}, both of which have a triplet multiplicity ($S = 1$). The most stable quintet, in contrast, lies 0.49 eV higher in energy and can therefore be eliminated as a candidate for the ground state. Both the D_{2h}- and D_{3d}-symmetric triplets show strongly prolate distortions from the idealized icosahedron, and in fact the D_{2h}-symmetric structure bears a striking resemblance to the X-ray data: the Mn–Pb distances split into three distinct sets of 2.91, 3.15, and 3.35 Å (cf. 2.90, 3.10, and 3.30 Å from X-ray), while the computed Pb–Pb separations range from 3.16 to 3.76 Å (cf. 3.10–3.75 Å from X-ray). In the D_{3d}-symmetric structure, in contrast, there are only two distinct Mn–Pb bond lengths, 2.94 Å and 3.33 Å (in a 6:6 ratio) while the Pb–Pb bond lengths range from 3.16 to 3.64 Å. Despite the subtle differences between the D_{2h}- and D_{3d}-symmetric structures, the gross features of the prolate distortion are very similar: the span of Pb–Pb and Mn–Pb distances is almost identical, as is the average Pb–Pb separation (~3.30 Å vs 3.22 Å from experiment). The second orientation of the D_{3d}-symmetric cluster anion shown in Figure 5 emphasizes the point that structural differences between the D_{3d} and D_{2h} structures are minimal. The D_{3d} isomer proves to be the global minimum although the D_{2h}-symmetric alternative lies only 0.02 eV higher in energy, well within the anticipated accuracy limits of the computation. In fact, the D_{2h}-symmetric structure is not a true minimum but rather represents a transition state (i18 cm^{-1}) which connects two equivalent D_{3d}-symmetric geometries. The magnitude of the imaginary frequency is, however, very small, and we conclude only that the potential energy surface is very flat in the region connecting D_{2h}- and D_{3d}-symmetric structures. No C_{2h}-symmetric minima were located; all attempts converged on the nearest D_{2h} -symmetric alternative. We have also located a perfectly icosahedral stationary point (Mn–Pb = 3.11 Å, Pb–Pb = 3.27 Å), which lies 0.64 eV above the D_{3d}-symmetric global minimum. The large energy gap indicates that the crystallographically observed prolate distortion has a strong intrinsic

Table 4. Calculated Bond Parameters, Energies, and Mulliken Spin Densities of $[Mn@Pb_{12}]^{3-}$ and $Ni@Pb_{12}$[a]

	$[Mn@Pb_{12}]^{3-}$				$Ni@Pb_{12}$			
	I_h	D_{2h}	D_{3d}	D_{5d}	I_h	D_{2h}	D_{3d}	D_{5d}
				Bond Parameters				
M−Pb (Å)	3.11 (12)	2.91, 3.15, 3.35 (4:4:4)	2.94, 3.33 (6:6)	2.92, 3.15 (2:10)	3.10 (12)	3.06, 3.10, 3.13 (4:4:4)	3.08, 3.12 (6:6)	3.09, 3.13 (2:10)
Pb−Pb (Å)	3.27 (30)	3.16, 3.17, 3.18, 3.22, 3.46, 3.76 (2:8:2:8:8:2)	3.16, 3.18, 3.26, 3.64 (6:6:12:6)	3.18, 3.28, 3.36 (6:6:6)	3.26 (30)	3.23, 3.25, 3.28, 3.29 (2:18:8:2)	3.24, 3.26, 3.27 (6:6:18)	3.25, 3.27 (20:10)
				Spin Densities				
M	3.21	3.35	3.33	3.18	0.63	0.68	0.71	0.66
ΣPb_{12}	−1.21	−1.35	−1.33	−1.18	1.37	1.32	1.29	1.34
				Energy (eV)				
	+0.64	+0.02	0.00	+0.32	+0.10	0.00	0.00	+0.04

[a] Values in parentheses indicate the number of symmetry equivalent bonds of a given length.

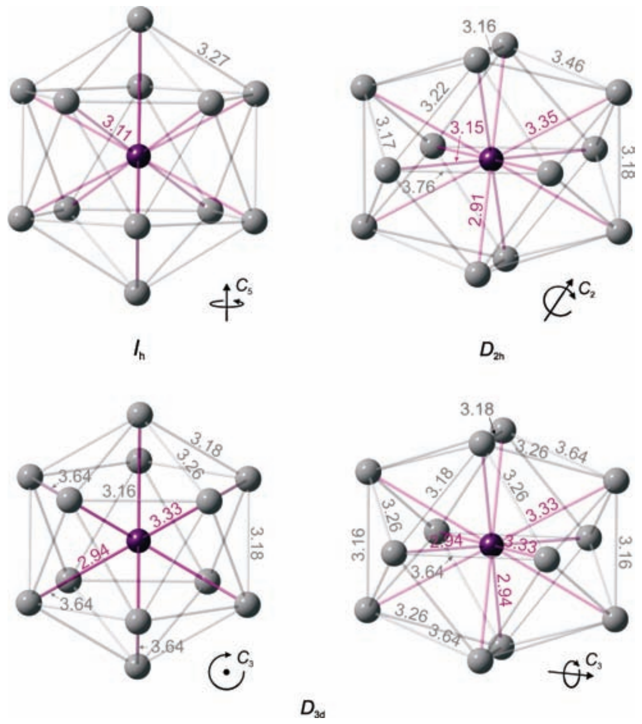

Figure 5. Optimized geometries of $[Mn@Pb_{12}]^{3-}$ (I_h, D_{2h}, and D_{3d} symmetries). Mn−Pb bonds and distances (Å) in purple, Pb−Pb bonds, and distances in gray. The orientation of the principal axis of rotation is indicated.

electronic driving force. Also included in Table 4 are the structural parameters, spin densities, and energies of the corresponding stationary points for the isoelectronic species $Ni@Pb_{12}$. Deng and co-workers have previously reported that the distortions from icosahedral symmetry in this species are small,[63] and our own calculations confirm this to be the case: the shortest and longest Ni−Pb distances differ by only 0.07 Å and the D_{2h}- and D_{3d}-symmetric structures are only 0.10 eV more stable than the perfectly icosahedral reference point.

Having established that DFT reproduces the key experimental observables for $[Mn@Pb_{12}]^{3-}$ (viz., the strong prolate distortion and the nonsinglet ground state), we are in a position to explore the electronic origins of the distortion. The perfectly icosahedral closed-shell species $[Ni@Pb_{12}]^{2-}$, the Kohn−Sham orbitals of which are shown in Figure 6, provides a natural reference point for the discussion. Eichhorn and co-workers have previously discussed the electronic structure of the platinum analogue, which is very similar, qualitatively and quantitatively.[2] The highest occupied molecular orbital (HOMO) and HOMO−1, $2h_g$ and $1t_{1u}$, are localized primarily on the Pb_{12} cage, the latter lying just above the 5-fold degenerate orbitals with dominant Ni 3d character ($1h_g$). The lowest unoccupied molecular orbital (LUMO) and LUMO+1 ($1g_g$ and $3h_g$, respectively) have almost exclusive Pb 6p character, and their spatial properties prove to be critical to the discussion of the low-symmetry distortion in $[Mn@Pb_{12}]^{3-}$: the LUMO is a linear combination of tangentially oriented 6p orbitals on Pb ("surface-only" orbitals in the nomenclature of King and co-workers).[64,65] In contrast the h_g-symmetric LUMO+1 can in principle have both radial and tangential character, but the contour plot in Figure 6 confirms that the radial component is dominant.

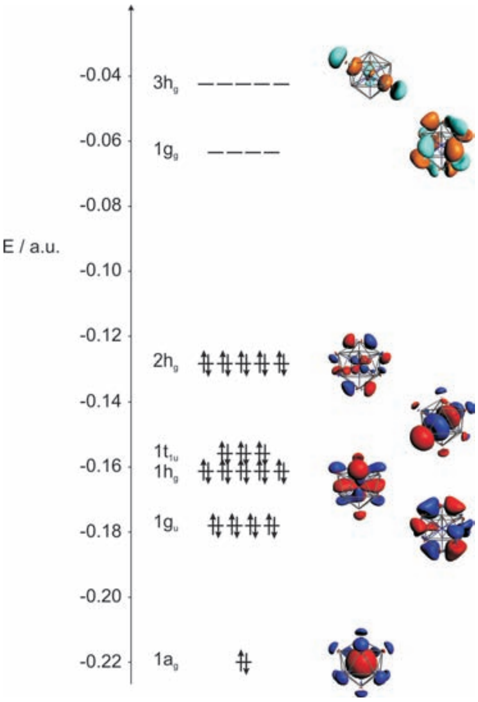

Figure 6. Kohn–Sham orbitals for icosahedral $[Ni@Pb_{12}]^{2-}$ (contour value 0.025 au). Only one component of each degenerate orbital is shown.

The removal of two electrons from the h_g-symmetric HOMO of $[Ni@Pb_{12}]^{2-}$ generates a Jahn–Teller instability, and thus distortion from the I_h symmetry of the closed-shell systems is to be anticipated. We note, however, that while this statement is equally true for both $[Mn@Pb_{12}]^{3-}$ and $Ni@Pb_{12}$, the nature and magnitude of the distortion is very different. The Kohn–Sham orbitals for $Ni@Pb_{12}$, in both I_h and D_{2h} symmetry, are shown in Figure 7. The two holes are localized in a primarily Pb-based HOMO, and the majority of the spin density is therefore distributed over the Pb_{12} cage ($\rho(Pb_{12}) = 1.37$) with only a small amount transferred onto the Ni center ($\rho(Ni) = 0.63$). The presence of same-spin (i.e., spin-α) density on *both* metal and ligand (in this case the Pb_{12} cage) is typical of cases where the dominant interaction is between the d orbitals of the metal and an occupied ligand-based donor orbital. The D_{2h}-symmetric form is only marginally more stable, and the frontier orbital domain and spin density distribution are not substantially affected by the distortion: the degeneracy of the $2h_g$ orbital is lifted such that a 3-below-2 pattern emerges, but the magnitude of the splitting is less than 0.01 au.

The frontier Kohn–Sham orbitals (Figure 8) and net spin densities (Table 4) for $[Mn@Pb_{12}]^{3-}$ (I_h and D_{2h}) indicate a very different electronic situation from the isoelectronic $Ni@Pb_{12}$. The net spin density on the Mn center (+3.21 in I_h symmetry) is much greater than that in $NiPb_{12}$ (+0.63) and even exceeds the limiting value of 2.0 for an entirely metal-centered triplet. To compensate for this high spin density at Mn, a negative (i.e., spin-β) density of -1.21 is delocalized over the Pb_{12} cage. The accumulation of minority-spin density on the ligand is very typical of ligand-centered radicals, which are most commonly found in combination with first row transition elements near the middle of the d block (Mn, Fe, Co).

The dramatically different electron density distributions in the Ni and Mn species can be traced to the relative stabilization of the 3d orbitals on moving left to right across the transition series. Thus the h_g-symmetric HOMO in I_h symmetry lies considerably higher in $[Mn@Pb_{12}]^{3-}$ than in $Ni@Pb_{12}$, and moreover has dominant Mn 3d rather than Pb 6p character. The complementary Pb 6p character is now localized in the lower-lying $1h_g$ orbital. As a result the holes in the valence shell (and therefore the unpaired electron density) are localized on the Mn center rather than over 12 Pb atoms, and the exchange splitting between spin-α and spin-β components of the $2h_g$ HOMO is much more pronounced. The combined effects of (i) the lower effective nuclear charge on Mn and (ii) the greater exchange splitting of the HOMO serve to push the spin-β component up, such that it lies in the same energetic window as the LUMO ($1g_g$) and LUMO +1 ($3h_g$) of the $[Pb_{12}]^{2-}$ cage. Symmetry-allowed mixing between the latter and the Mn 3d orbitals therefore results in partial transfer of spin-β electron density from the metal to the cage. The resultant build-up of spin-α density on the metal means that $\rho(Mn)$ exceeds the value of 2.0 for a pure metal-centered triplet.

The impact of allowing the structure to relax from I_h to D_{2h} symmetry is energetically much more significant in $[Mn@Pb_{12}]^{3-}$ compared to $Ni@Pb_{12}$ (0.62 eV vs 0.10 eV), and the perturbations to the frontier orbitals are similarly magnified. Thus three components of the spin-β $2h_g$ HOMO are stabilized by more than 0.02 au while the other two are destabilized by ~0.02 au. The origin of this much enhanced splitting, and hence much more pronounced asymmetry of the cluster, lies in the energetic proximity of the LUMO and LUMO +1 of the cage ($1g_g$ and $2h_g$, respectively). The two orbitals are spatially very different: the former has exclusive tangential Pb 6p character while the 6p orbitals in the latter are aligned primarily in the radial direction. In I_h symmetry, sharing of d-electron density between the metal and the cage occurs exclusively through the h_g orbitals, and the result is the presence of radial Pb 6p character in the partially occupied $2h_g(\beta)$ orbital (Figure 8a). Low-symmetry distortions, however, allow second-order mixing of one or more components of the closely separated h_g and g_g sets, the net effect of which is to introduce some strongly Pb–Pb antibonding tangential character from the g_g manifold into the highest-lying occupied spin-β orbitals. A comparison of the contour plots of the spin-β HOMOs shown in Figures 8a and 8b highlights the tangential nature of the Pb_{12}-based components of the HOMO in D_{2h} symmetry. The net effect of this second-order mixing is to further enhance charge transfer from the endohedral manganese center to the $[Pb_{12}]^{2-}$ cage, increasing the magnitude of the spin densities by ±0.14 ($\rho(Mn) = +3.35$, $\rho(Pb_{12}) = -1.35$) and allowing the Mn center to approach more closely the limit of the half-filled shell. The descent in symmetry summarized in Table 5 also highlights the fact that the D_{2h} and D_{3d}-symmetric distortions allow for stabilization of three of the five components of the h_g-symmetric orbital, precisely the situation required for a formal d^8 electron count with three spin-β electrons. A D_{5d}-symmetric distortion, in contrast, allows only for the stabilization of two (either e_{1g} or e_{2g}) or four (both e_{1g} and e_{2g}) components but not three, and indeed the corresponding optimized structure is stabilized by only 0.32 eV relative to the I_h-symmetric reference state. In the isoelectronic $Ni@Pb_{12}$ analogue, where transfer of electron density from the endohedral metal to the Pb_{12} cage is much less pronounced, the energetic distinction between I_h, D_{5d}, and D_{2h}/D_{3d} structures is much more marginal.

The "broken-symmetry" nature of the wave function for $[Mn@Pb_{12}]^{3-}$, where spin-α and spin-β orbitals differ spatially, is very typical of ligand-centered radicals, which, as noted above,

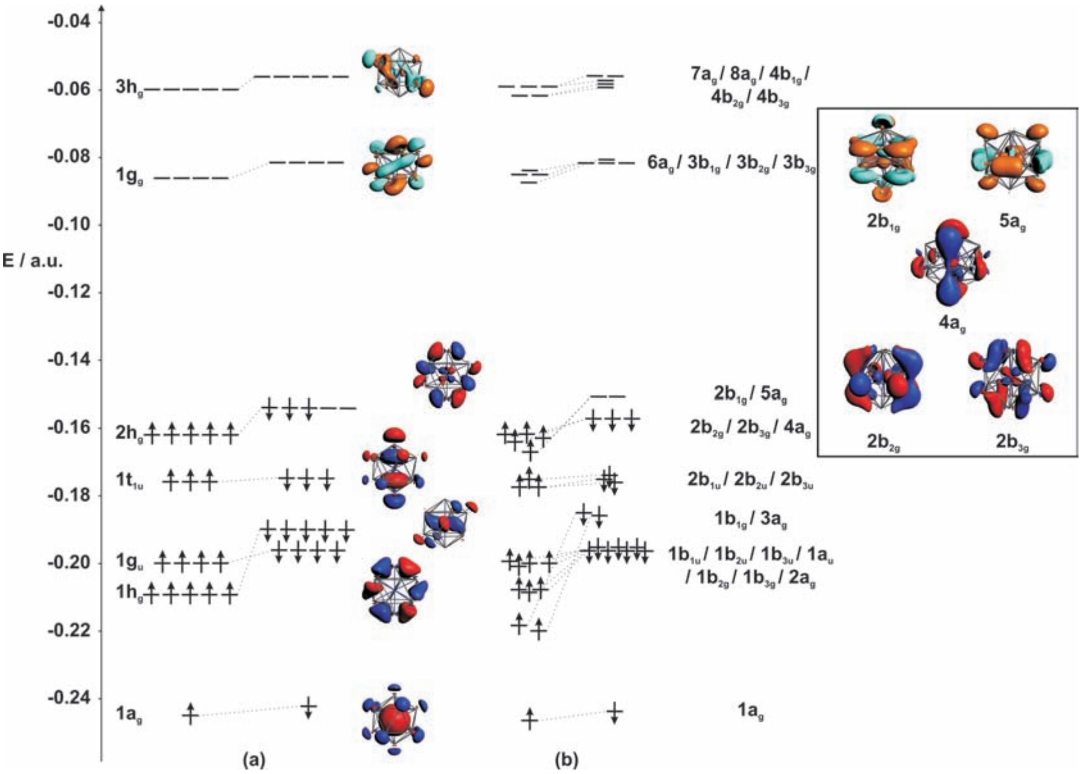

Figure 7. Kohn–Sham orbitals for Ni@Pb_{12} in (a) I_h and (b) D_{2h} symmetry (contour value 0.025 au). Inset are contour plots of the five frontier orbitals (3 occupied, 2 vacant) of the spin-β manifold in D_{2h} symmetry.

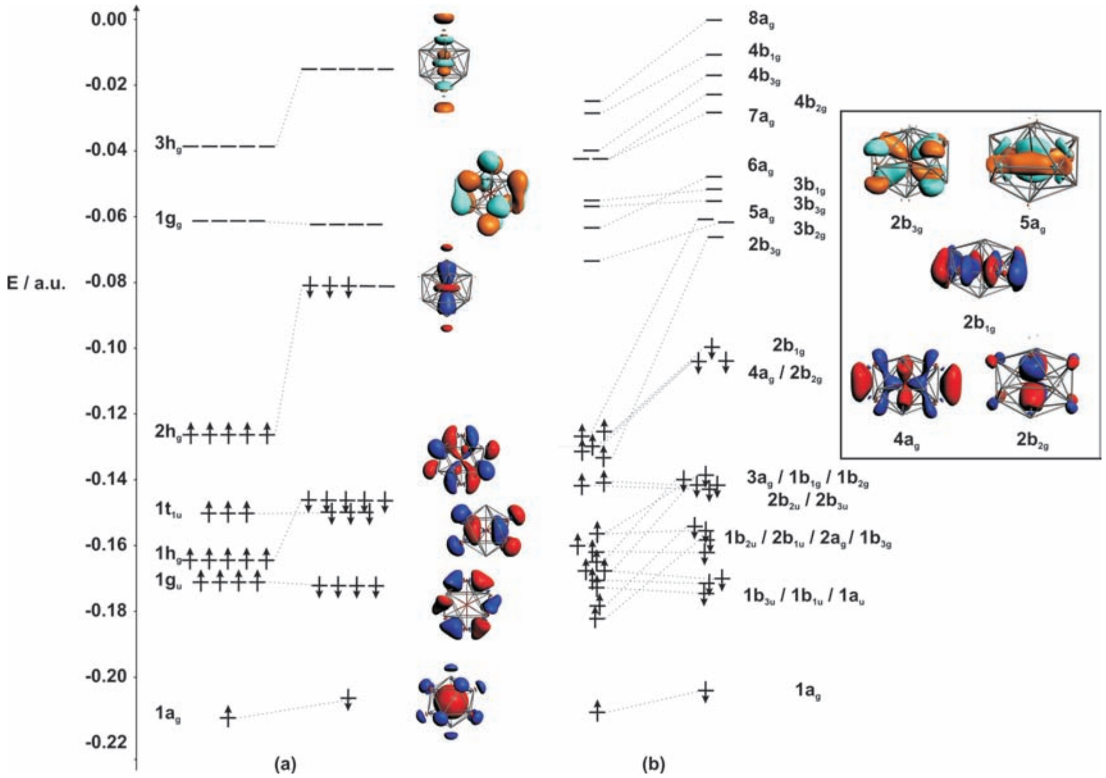

Figure 8. Kohn–Sham orbitals (β-spin manifold) for $[Mn@Pb_{12}]^{3-}$ in (a) I_h and (b) D_{2h} symmetry (contour value 0.025 au). Inset are contour plots of the five frontier orbitals (3 occupied, 2 vacant) of the spin-β manifold in D_{2h} symmetry.

Table 5. Descent in Symmetry $I_h \rightarrow D_{5d} \rightarrow D_{3d} \rightarrow D_{2h}$

I_h	D_{5d}	D_{3d}	D_{2h}
g_g	$e_{1g} + e_{2g}$	$e_g + a_{1g} + a_{2g}$	$a_g + b_{1g} + b_{2g} + b_{3g}$
h_g	$e_{1g} + e_{2g} + a_{1g}$	$2e_g + a_{1g}$	$2a_g + b_{1g} + b_{2g} + b_{3g}$

are most common for transition metals near the middle of the 3d block. The reason for this is that the high exchange energies associated with half-filled (or nearly half-filled) shell disfavor the sharing of electron density between metal and ligand. We can therefore identify the driving force pushing spin-β electron density onto the Pb_{12} cage as the increased exchange stabilization associated with the accumulation of spin-α density at the metal. The limit of complete transfer of the three electrons to the cage corresponds to a $[Mn(II)@Pb_{12}{}^{5-}]^{3-}$ distribution with a stable half-filled Mn d shell, consistent with the proposals of Deng et al.[63] and Kumar et al.[52] for $[Mn(II)@E_{12}{}^{2-}]$. Alternatively, and by analogy to Fässler's iridium system,[4] the cluster could be formulated as $[Mn(-I)@Pb_{12}{}^{2-}]^{3-}$. The net spin densities of +3.21 and −1.21 on Mn and the Pb_{12} cage, respectively (Table 4), lie approximately midway between the values anticipated for the two limiting forms: $[Mn(II)@Pb_{12}{}^{5-}]^{3-}$ ($\rho(Mn) = +5.0$, $\rho(Pb_{12}) = -3.0$) and $[Mn(-I)@Pb_{12}{}^{2-}]^{3-}$ ($\rho(Mn) = +2.0$, $\rho(Pb_{12}) = 0.0$).

6. CONCLUSIONS

In this manuscript we have reported the isolation and characterization of the first example of an open-shell metal-centered deltahedral cluster anion, $[Mn@Pb_{12}]^{3-}$. A combined experimental and computational analysis suggests that the pronounced structural distortion away from icosahedral symmetry in the solid-state is the result of substantial electron transfer from the formally Mn(−I) center to the $[Pb_{12}]^{2-}$ cage. While this conclusion appears rather surprising in light of the formal electron deficiency of the 34 electron cluster, we note that in transition elements near the middle of the d block, particularly those in the first row, there is a strong driving force toward formation of a half-filled rather than filled d shell. Thus $[Mn@Pb_{12}]^{3-}$ is most appropriately viewed not as an electron deficient 34 electron cluster with a d-electron count two fewer than the 36 electrons required for a closed shell configuration, but rather as a very electron rich system with three electrons more than the 31 required to complete a closed shell on the $[Pb_{12}]^{2-}$ cage and a half-filled shell at the metal center. The isolation of the $[Mn@Pb_{12}]^{3-}$ anion therefore raises the real possibility of an extensive chemistry based on the so-called "magnetic superatoms" where a paramagnetic half-filled shell is trapped inside a diamagnetic cage.

■ ASSOCIATED CONTENT

Ⓢ **Supporting Information.** X-ray crystallographic files in CIF format for **1a** and **1b**. Full experimental and computational details as well as a complete literature citation for ref 37c are also available. This material is available free of charge via the Internet at http://pubs.acs.org.

■ AUTHOR INFORMATION

Corresponding Author

*E-mail: john.mcgrady@chem.ox.ac.uk (J.M.), jose.goicoechea@chem.ox.ac.uk (J.M.G.).

■ ACKNOWLEDGMENT

We thank the EPSRC and the University of Oxford (studentships to B.Z. and T.K.) for financial support of this research. We also thank Dr. Mark S. Denning for the synthesis of K_4Pb_9, Stephen Boyer (London Metropolitan University) for the elemental analyses, Dr. Jeffrey Harmer and Mark Irwin for their assistance with EPR spectroscopy, and the University of Oxford for access to OSC and CAESR facilities. Finally, we also thank Diamond Light Source for beam-time on I19 (MT1858) and Dr. Kirsten E. Christensen and Dr. David R. Allan for their assistance with data collection and refinement on sample **1b**.

■ REFERENCES

(1) For recent reviews see: (a) Sevov, S. C.; Goicoechea, J. M. *Organometallics* **2006**, *25*, 5678. (b) Scharfe, S.; Fässler, T. F. *Phil. Trans. R. Soc. A* **2010**, *368*, 1265.

(2) Esenturk, E. N.; Fettinger, J.; Lam, Y.-F.; Eichhorn, B. *Angew. Chem., Int. Ed.* **2004**, *43*, 2132.

(3) Esenturk, E. N.; Fettinger, J.; Eichhorn, B. W. *J. Am. Chem. Soc.* **2006**, *128*, 9178.

(4) Wang, J.-Q.; Stegmaier, S.; Wahl, B.; Fässler, T. F. *Chem.—Eur. J.* **2010**, *16*, 1793.

(5) Zhang, X.; Li, G.; Xing, X.; Zhao, X.; Tang, Z.; Gao, Z. *Rapid. Commun. Mass Spectrom.* **2001**, *15*, 2399.

(6) Neukermans, S.; Wang, X.; Veldeman, N.; Janssens, E.; Silverans, R. E.; Lievens, P. *Int. J. Mass Spectrom.* **2006**, *252*, 145.

(7) Goicoechea, J. M.; Sevov, S. C. *J. Am. Chem. Soc.* **2006**, *128*, 4155.

(8) Scharfe, S.; Fässler, T. F.; Stegmaier, S.; Hoffmann, S. D.; Ruhland, K. *Chem.—Eur. J.* **2008**, *14*, 4479.

(9) Esenturk, E. N.; Fettinger, J.; Eichhorn, B. W. *Chem. Commun.* **2005**, 247.

(10) (a) Wang, J.-Q.; Stegmaier, S.; Fässler, T. F. *Angew. Chem., Int. Ed.* **2009**, *48*, 1998. (b) Zhou, B.; Denning, M. S.; Kays, D. L.; Goicoechea, J. M. *J. Am. Chem. Soc.* **2009**, *131*, 2802.

(11) Goicoechea, J. M.; Sevov, S. C. *Angew. Chem., Int. Ed.* **2005**, *44*, 4026.

(12) Goicoechea, J. M.; Sevov, S. C. *J. Am. Chem. Soc.* **2005**, *127*, 7676.

(13) (a) Sun, Z. M.; Xiao, H.; Li, J.; Wang, L.-S. *J. Am. Chem. Soc.* **2007**, *129*, 9560. (b) Kocak, F. S.; Zavalij, P.; Lam, Y.-F.; Eichhorn, B. W. *Inorg. Chem.* **2008**, *47*, 3515.

(14) Kesanli, B.; Halsig, J. E.; Zavalij, P.; Fettinger, J. C.; Lam, Y.-F.; Eichhorn, B. W. *J. Am. Chem. Soc.* **2007**, *129*, 4567.

(15) (a) Hull, M. W.; Sevov, S. C. *Inorg. Chem.* **2007**, *46*, 10953. (b) Chapman, D. J.; Sevov, S. C. *Inorg. Chem.* **2008**, *47*, 6009. (c) Hull, M. W.; Sevov, S. C. *J. Am. Chem. Soc.* **2009**, *131*, 9026. (d) Gillett-Kunnath, M. M.; Petrov, I.; Sevov, S. C. *Inorg. Chem.* **2010**, *49*, 721.

(16) (a) Ugrinov, A.; Sevov, S. C. *J. Am. Chem. Soc.* **2002**, *124*, 2442. (b) Ugrinov, A.; Sevov, S. C. *J. Am. Chem. Soc.* **2003**, *125*, 14059. (c) Ugrinov, A.; Sevov, S. C. *Chem.—Eur. J.* **2004**, *10*, 3727. (d) Hull, M. W.; Sevov, S. C. *Angew. Chem., Int. Ed.* **2007**, *46*, 6695. (e) Eichhorn, B. W.; Haushalter, R. C.; Pennington, W. T. *J. Am. Chem. Soc.* **1988**, *110*, 8704. (f) Eichhorn, B. W.; Haushalter, R. C. *Chem. Commun.* **1990**, 937. (g) Campbell, J.; Mercier, H. P. A.; Franke, H.; Santry, D. P.; Dixon, D. A.; Schrobilgen, G. J. *Inorg. Chem.* **2002**, *41*, 86. (h) Kesanli, B.; Fettinger, J.; Eichhorn, B. *Chem.—Eur. J.* **2001**, *7*, 5277. (i) Yong, L.; Hoffmann, S. D.; Fässler, T. F. *Eur. J. Inorg. Chem.* **2005**, 3663. (j) Esenturk, E. N.; Fettinger, J.; Eichhorn, B. *Polyhedron* **2006**, *25*, 521. (k) Kesanli, B.; Fettinger, J.; Gardner, D. R.; Eichhorn, B. *J. Am. Chem. Soc.* **2002**, *124*, 4779. (l) Goicoechea, J. M.; Sevov, S. C. *Organometallics* **2006**, *25*, 4530. (m) Zhou, B.; Denning, M. S.; Jones, C.; Goicoechea, J. M. *Dalton Trans.* **2009**, 1571. (n) Zhou, B.; Denning, M. S.; Chapman, T. A. D.; Goicoechea, J. M. *Inorg. Chem.* **2009**, *48*, 2899. (o) Downing, D. O.; Zavalij, P.; Eichhorn, B. W. *Eur. J. Inorg. Chem.* **2010**, 890.

(17) (a) Xu, L.; Sevov, S. C. *J. Am. Chem. Soc.* **1999**, *121*, 9245. (b) Hauptmann, R.; Fässler, T. F. *Z. Anorg. Allg. Chem.* **2003**, *629*, 2266. (c) Suchentrunk, C.; Daniels, J.; Somer, M.; Carrillo-Cabrera, W.; Korber, N. *Z. Naturforsch.* **2005**, *60b*, 277. (d) Ugrinov, A.; Sevov, S. C. *J. Am. Chem. Soc.* **2002**, *124*, 10990. (e) Yong, L.; Hoffmann, S. D.; Fässler, T. F. *Z. Anorg. Allg. Chem.* **2005**, *631*, 1149. (f) Ugrinov, A.; Sevov, S. C. *Inorg. Chem.* **2003**, *42*, 5789. (g) Yong, L.; Hoffmann, S. D.; Fässler, T. F. *Z. Anorg. Allg. Chem.* **2004**, *630*, 1977. (h) Downie, C.; Tang, Z.; Guloy, A. M. *Angew. Chem., Int. Ed.* **2000**, *39*, 338. (i) Downie, C.; Mao, J.-G.; Parmar, H.; Guloy, A. M. *Inorg. Chem.* **2004**, *43*, 1992. (j) Ugrinov, A.; Sevov, S. C. *C. R. Chim.* **2005**, *8*, 1878.

(18) Joseph, S.; Hamberger, M.; Mutzbauer, F.; Härtl, O.; Meier, M.; Korber, N. *Angew. Chem., Int. Ed.* **2009**, *48*, 8770.

(19) Nienhaus, A.; Hauptmann, R.; Fässler, T. F. *Angew. Chem., Int. Ed.* **2002**, *41*, 3213.

(20) Boeddinghaus, M. B.; Hoffmann, S. D.; Fässler, T. F. *Z. Anorg. Allg. Chem.* **2007**, *633*, 2338.

(21) Denning, M. S.; Goicoechea, J. M. *Dalton Trans.* **2008**, 5882.

(22) Spiekermann, A.; Hoffmann, S. D.; Kraus, F.; Fässler, T. F. *Angew. Chem., Int. Ed.* **2007**, *46*, 1638.

(23) Spiekermann, A.; Hoffmann, S. D.; Fässler, T. F.; Krossing, I.; Preiss, U. *Angew. Chem., Int. Ed.* **2007**, *46*, 5310.

(24) Yong, L.; Boeddinghaus, M. B.; Fässler, T. F. *Z. Anorg. Allg. Chem.* **2010**, *636*, 1293.

(25) Zhou, B.; Denning, M. S.; Chapman, T. A. D.; McGrady, J. E.; Goicoechea, J. M. *Chem. Commun.* **2009**, 7221.

(26) (a) Böhme, B.; Guloy, A.; Tang, Z.; Schnelle, W.; Burkhardt, U.; Baitinger, M.; Grin, Y. *J. Am. Chem. Soc.* **2007**, *129*, 5348. (b) Guloy, A. M.; Ramlau, R.; Tang, Z.; Schnelle, W.; Baitinger, M.; Grin, Y. *Nature* **2006**, *443*, 320. (c) Armatas, G. S.; Kanatzidis, M. G. *Nature* **2006**, *441*, 1122. (d) Armatas, G. S.; Kanatzidis, M. G. *Science* **2006**, *313*, 817. (e) Armatas, G. S.; Kanatzidis, M. G. *J. Am. Chem. Soc.* **2008**, *130*, 11430. (f) Sun, D.; Riley, A. E.; Cadby, A. J.; Richman, E. K.; Korlann, S. D.; Tolbert, S. H. *Nature* **2006**, *441*, 1126. (g) Chandrasekharan, N.; Sevov, S. C. *J. Electrochem. Soc.* **2010**, *157*, C140.

(27) Spiekermann, A.; Hoffmann, S. D.; Fässler, T. F. *Angew. Chem., Int. Ed.* **2006**, *45*, 3459.

(28) Zhou, B.; Goicoechea, J. M. *Chem.—Eur. J.* **2010**, *16*, 11145.

(29) Rios, D.; Sevov, S. C. *Inorg. Chem.* **2010**, *49*, 6396.

(30) (a) Wade, K. *J. Adv. Inorg. Chem. Radiochem.* **1976**, *18*, 1. (b) Wade, K. *J. Chem. Soc., D* **1971**, 792. (c) Mingos, D. M. P. *Nat. Phys. Sci.* **1972**, *99*, 236. (d) Mingos, D. M. P. *Acc. Chem. Res.* **1984**, *17*, 311.

(31) Queneau, V.; Sevov, S. C. *Inorg. Chem.* **1998**, *37*, 1358.

(32) (a) Gambarotta, S.; Floriani, C.; Chiesi-Villa, A.; Guastini, C. *Chem. Commun.* **1983**, 1128. (b) Solari, E.; Musso, F.; Gallo, E.; Floriani, C.; Re, N.; Chiesi-Villa, A.; Rizzoli, C. *Organometallics* **1995**, *14*, 2265.

(33) Cosier, J.; Glazer, A. M. *J. Appl. Crystallogr.* **1986**, *19*, 105.

(34) Otwinowski, Z.; Minor, W. Processing of X-ray Diffraction Data Collected in Oscillation Mode. In *Methods in Enzymology*; Academic Press: New York, 1997.

(35) *CrystalClear-SM Expert 2.0 r4*; Rigaku Corp.: The Woodlands, TX, 2009.

(36) Sheldrick, G. M. *Acta Crystallogr.* **2008**, *A64*, 112.

(37) (a) te Velde, G.; Bickelhaupt, F. M.; Baerends, E. J.; Fonseca Guerra, C.; van Gisbergen, S. J. A.; Snijders, J. G.; Ziegler, T. *J. Comput. Chem.* **2001**, *22*, 931. (b) Fonseca Guerra, C.; Snijders, J. G.; te Velde, G.; Baerends, E. J. *Theor. Chem. Acc.* **1998**, *99*, 391.(c) Baerends, E. J.; et al. *ADF2009.01*; SCM, Theoretical Chemistry, Vrije Universiteit: Amsterdam, The Netherlands; http://www.scm.com.

(38) Parr, R. G.; Yang, W. *Density Functional Theory of Atoms and Molecules*; Oxford University Press: Oxford, England, 1989.

(39) Vosko, S. H.; Wilk, L.; Nusair, M. *Can. J. Phys.* **1980**, *58*, 1200.

(40) (a) Becke, A. D. *Phys. Rev. A.* **1988**, *38*, 3098. (b) Perdew, J. P. *Phys. Rev. B* **1986**, *33*, 8822.

(41) (a) van Lenthe, E.; Baerends, E. J.; Snijders, J. G. *J. Chem. Phys.* **1993**, *99*, 4597. (b) van Lenthe, E.; Baerends, E. J.; Snijders, J. G. *J. Chem. Phys.* **1994**, *101*, 9783. (c) van Lenthe, E.; Ehlers, A. E.; Baerends, E. J. *J. Chem. Phys.* **1999**, *110*, 8943.

(42) Klamt, A. *J. Phys. Chem.* **1995**, *99*, 2224.

(43) Versluis, L.; Ziegler, T. *J. Chem. Phys.* **1988**, *88*, 322.

(44) Pauling, L. *Proc. Natl. Acad. Sci. U.S.A.* **1975**, *72*, 3799.

(45) Fässler, T. F.; Hunziker, M.; Spahr, M. E.; Lueken, H.; Schilder, H. *Z. Anorg. Allg. Chem.* **2000**, *626*, 692.

(46) Hiura, H.; Miyazaki, T.; Kanayama, T. *Phys. Rev. Lett.* **2001**, *86*, 1733.

(47) Lu, J.; Nagase, S. *Phys. Rev. Lett.* **2003**, *90*, 115506.

(48) Hagelberg, F.; Xiao, C.; Lester, W. A. *Phys. Rev. B* **2003**, *67*, 035426.

(49) Sen, P.; Mitas, L. *Phys. Rev. B* **2003**, *68*, 155404.

(50) Sun, Q.; Wang, Q.; Briere, T. M.; Kumar, V.; Kawazoe, Y.; Jena, P. *Phys.Rev. B* **2002**, *65*, 235417.

(51) Kumar, V.; Kawazoe, Y. *App. Phys. Lett.* **2003**, *83*, 2677.

(52) Kumar, V.; Singh, A. K.; Kawazoe, Y. *Nano Lett.* **2004**, *4*, 677.

(53) King, R. B.; Silaghi-Dumitrescu, I.; Uţă, M. M. *Chem.—Eur. J.* **2008**, *14*, 4542.

(54) King, R. B.; Silaghi-Dumitrescu, I.; Uţă, M. M. *J. Phys Chem. A* **2009**, *113*, 527.

(55) Kumar, V.; Kawazoe, Y. *App. Phys. Lett.* **2002**, *80*, 859.

(56) Lu, J.; Nagase, S. *Chem. Phys. Lett.* **2003**, *372*, 394.

(57) Neukermans, S.; Janssens, E.; Chen, Z. F.; Silverans, R. E.; Schleyer, P. v. R.; Lievens, P. *Phys. Rev. Lett.* **2004**, *92*, 163401.

(58) Rajesh, C.; Majumder, C. *Chem. Phys. Lett.* **2006**, *430*, 101.

(59) Rajesh, C.; Majumder, C. *J. Chem. Phys.* **2008**, *128*, 24308.

(60) Dognon, J. P.; Clavaguéra, C.; Pyykkö, P. *Angew. Chem., Int. Ed.* **2007**, *46*, 1427.

(61) Chen, D. L.; Tian, W. Q.; Lu, W. C.; Sun, C. C. *J. Chem. Phys.* **2006**, *124*, 154313.

(62) Cui, L.-F.; Huang, X.; Wang, L.-M.; Li, J.; Wang, L.-S. *J. Phys. Chem. A* **2006**, *110*, 10169.

(63) Chen, X.; Deng, K.; Liu, Y.; Tang, C.; Yuan, Y.; Hu, F.; Wu, H.; Huang, D.; Tan, W.; Wang, X. *Chem. Phys. Lett.* **2008**, *462*, 275.

(64) King, R. B. *Inorg. Chem.* **1988**, *27*, 1941.

(65) King, R. B. *J. Comput. Chem.* **1987**, *8*, 341.